Electronic Supplementary Material (ESI) for Physical Chemistry Chemical Physics.

Electronic Supplementary Information

Spin Hall effect of transmitted light through α-Li_3N-type topological semimetals

Guang-Yi Jia,[1,*] Rui-Xia Zhang,[1] Ting Tang,[2] Qian Li,[1] Ali Ebrahimian,[3] Zahra Torbatian,[4] Reza Asgari[3,†]

[1]*School of Science, Tianjin University of Commerce, Tianjin 300134, P.R. China*

[2]*Tianjin Key Laboratory of Refrigeration Technology, Tianjin University of Commerce, Tianjin 300134, P.R. China*

[3]*School of Physics, Institute for Research in Fundamental Sciences, IPM, Tehran 19395-5531, Iran*

[4]*School of Nano Science, Institute for Research in Fundamental Sciences, IPM, Tehran 19395-5531, Iran*

E-mails: *gyjia87@163.com; †asgari@ipm.ir

I. Ab Initio Calculations

A. Calculation Methods

In this study, for the sake of accurateness, structural optimization and electronic structure calculations are carried out using the all-electron full potential linearized augmented plane wave (FP-LAPW) method, as implemented in Exciting code [1]. The exchange-correlation potential is treated within the generalized gradient approximation of Perdew-Burke-Ernzerhof (PBE) [2]. In order to check the possible underestimation of the band gap within the PBE functional, hybrid density functional (HSE06) [3,4] is also employed. A $20 \times 20 \times 20$ Monkhorst-pack k-point mesh is properly used in the computations. All the structures are fully relaxed until the maximum residual force on each atom is less than 10^{-4} eVÅ^{-1}. The optimized lattice constants of Li_3N, Li_2KN, and Na_3N are $a = b = 3.648$ Å and $c = 3.885$ Å, $a = b = 3.713$ Å and $c = 5.701$ Å, $a = b = 4.488$ Å and $c = 4.660$ Å, respectively. The interstitial plane wave vector cut off K_{Max} is chosen in a way that $R_{MT}K_{Max}$ equals 8. The G_{Max} parameter is taken to be 14 Bohr^{-1}. The hole doping induced in α-Li_3N is simulated by shifting the Fermi level downward according to a standard rigid-band model. The influences of excitonic effects are important in order to correctly account for quantitative as well as qualitative features of optical spectra of Li_3N. Therefore, to include the electron-hole interaction, being absent in the random phase approximation, we apply many-body perturbation theory on top of the DFT calculations. The Bethe-Salpeter Equation for two-particles Green's function [5,6] is solved using the Exciting code. The matrix eigenvalue form of BSE is thus given by [7-9]

$$\sum_{v'c'k'} H_{vck,v'c'k'} A^{\lambda}_{v'c'k'} = E^{\lambda} A^{\lambda}_{vck}$$

where v, c, and k indicate the valence band, conduction band, and k-points in the reciprocal space, respectively. Eigenvalues E^{λ} and eigenvectors A^{λ}_{vck} represent the excitation energy of the jth-correlated electron-hole pair and the coupling coefficients used to construct the exciton wave function, respectively. The optical properties of semimetal structures are considered via using time-dependent density-functional theory (TDDFT) [10]. The inverse dielectric matrix is related to the susceptibility χ by the relation $\varepsilon^{-1}(q, \omega) = 1 + v(q)\chi(q, \omega)$, where v(q) is the bare Coulomb potential. In TDDFT, the susceptibility χ(q, ω) is obtained by making use of the linear response to TDDFT through the solution of Dyson equation

$$\chi(q, \omega) = \chi_0(q, \omega) + \chi_0(q, \omega)[v(q) + f_{xc}(q)]\chi(q, \omega)$$

where $\chi_0(q, \omega)$ is the KS susceptibility expressed in terms of the KS eigenvalues and eigenfunctions, $f_{xc}(q)$ is the exchange-correlation kernel, for which we make use of the adiabatic local-density approximation (ALDA). To study the convergence of the excitonic features in the optical properties, for all structures, the dielectric function has been calculated for different numbers of k-point. The momentum matrix elements for the optical properties have been converged using 30×30×30 k-points. In fact, the excitation energies converged within 70 meV.

B. Electronic Band Structures of Li_3N, Na_3N and Li_2KN

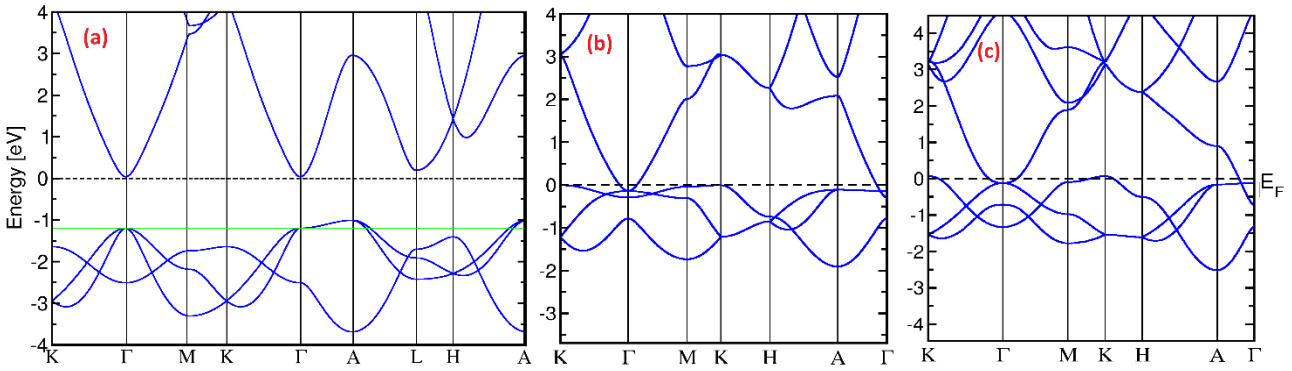

Fig. S1 The calculated bulk electronic band structure of (a) Li_3N, (b)Na_3N and (c)Li_2KN in PBE. The value of Fermi energy for hole-doped (0.1 holes/u.c.) Li_3N is shown by a green solid line in (a).

II. Complex Permittivities and Related Optical Spectra

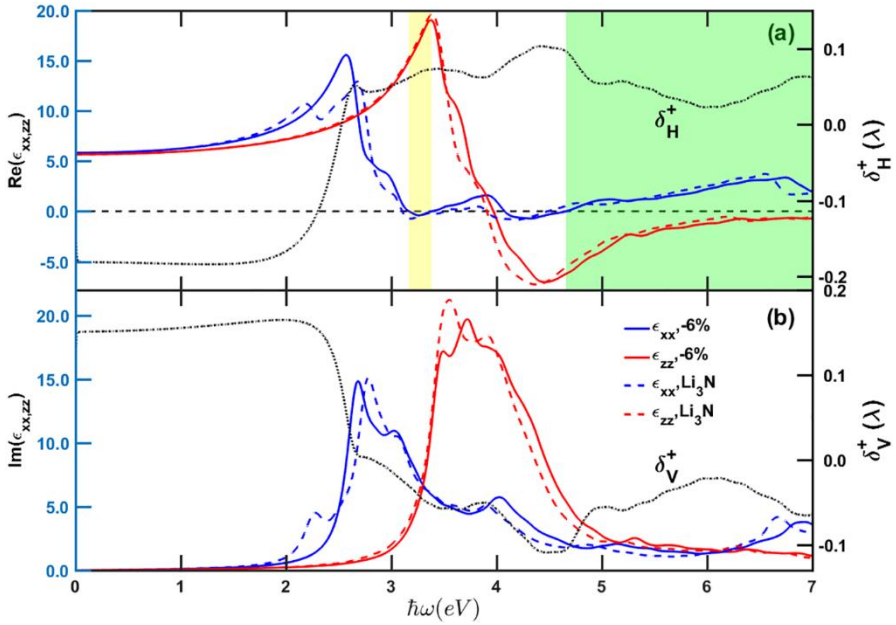

Fig. S2 (a) Real and (b) imaginary parts of the in-plane (ε_{xx}) and the out-of-plane (ε_{zz}) components of the relative permittivities for Li_3N and -6% strained Li_3N. The green and yellow areas indicate the photon energy ranges of type-I and type-II hyperbolic properties for -6% strained Li_3N, respectively. For comparison, the spectra of spin Hall shifts δ_H^+ and δ_V^+ at $\theta_i = 10^o$ for -6% strained Li_3N are shown by dot lines.

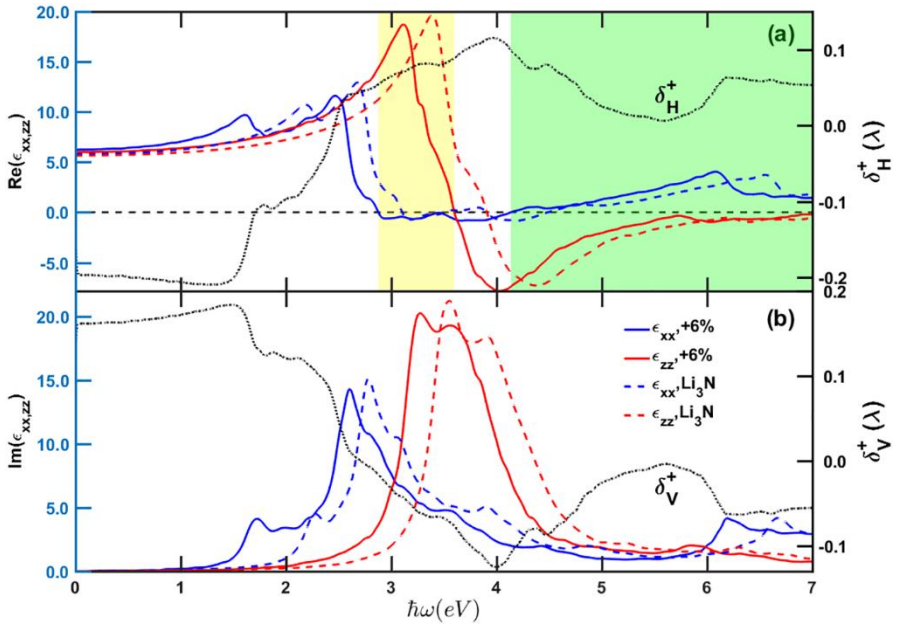

Fig. S3 (a) Real and (b) imaginary parts of the in-plane (ε_{xx}) and the out-of-plane (ε_{zz}) components of the relative permittivities for Li_3N and +6% strained Li_3N. The green and yellow areas indicate the photon energy ranges of type-I and type-II hyperbolic properties for +6% strained Li_3N, respectively. For comparison, the spectra of spin Hall shifts δ_H^+ and δ_V^+ at $\theta_i = 10^o$ for +6% strained Li_3N are shown by dot lines.

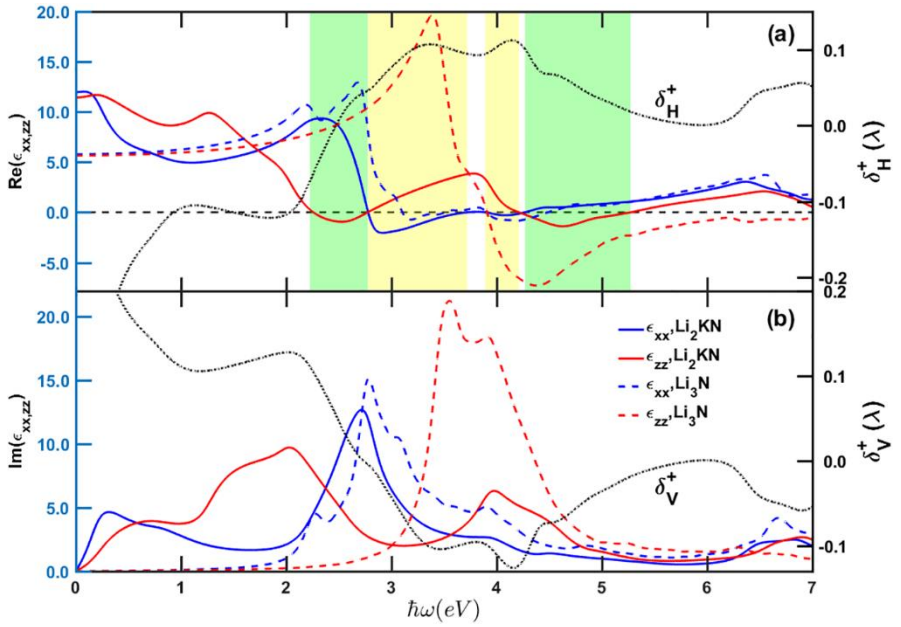

Fig. S4 (a) Real and (b) imaginary parts of the in-plane (ε_{xx}) and the out-of-plane (ε_{zz}) components of the relative permittivities for Li_3N and Li_2KN. The green and yellow areas indicate the photon energy ranges of type-I and type-II hyperbolic properties for Li_2KN, respectively. The dielectric function of Li_2KN incorporates only the interband contribution and the intraband contribution is ignored here. For comparison, the spectra of spin Hall shifts δ_H^+ and δ_V^+ at $\theta_i = 10^o$ for Li_2KN are shown by dot lines.

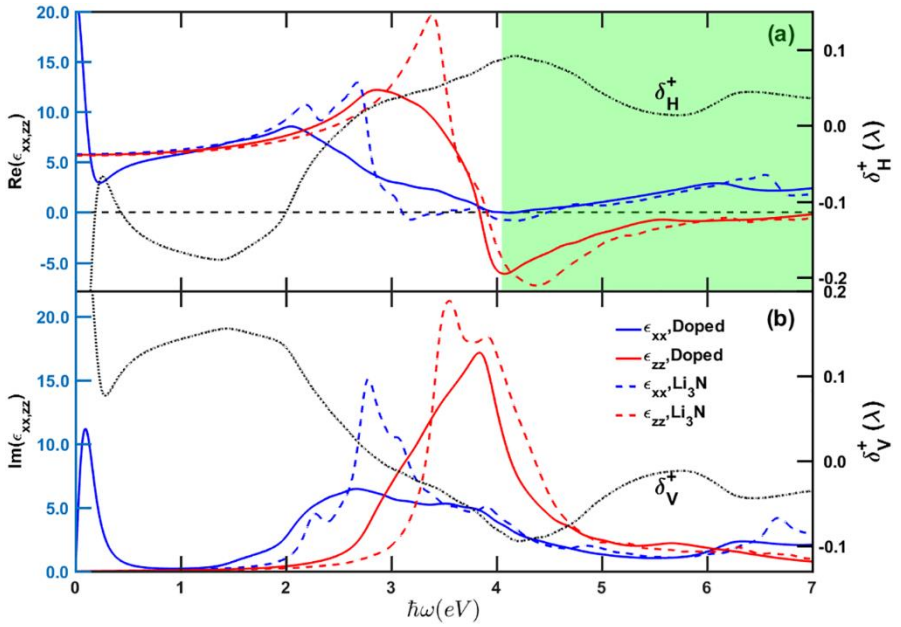

Fig. S5 (a) Real and (b) imaginary parts of the in-plane (ε_{xx}) and the out-of-plane (ε_{zz}) components of the relative permittivities for Li_3N and hole-doped Li_3N. The green area indicates the photon energy range of type-I hyperbolic property for hole-doped Li_3N. For comparison, the spectra of spin Hall shifts δ_H^+ and δ_V^+ at $\theta_i = 10^o$ for hole-doped Li_3N are shown by dot lines.

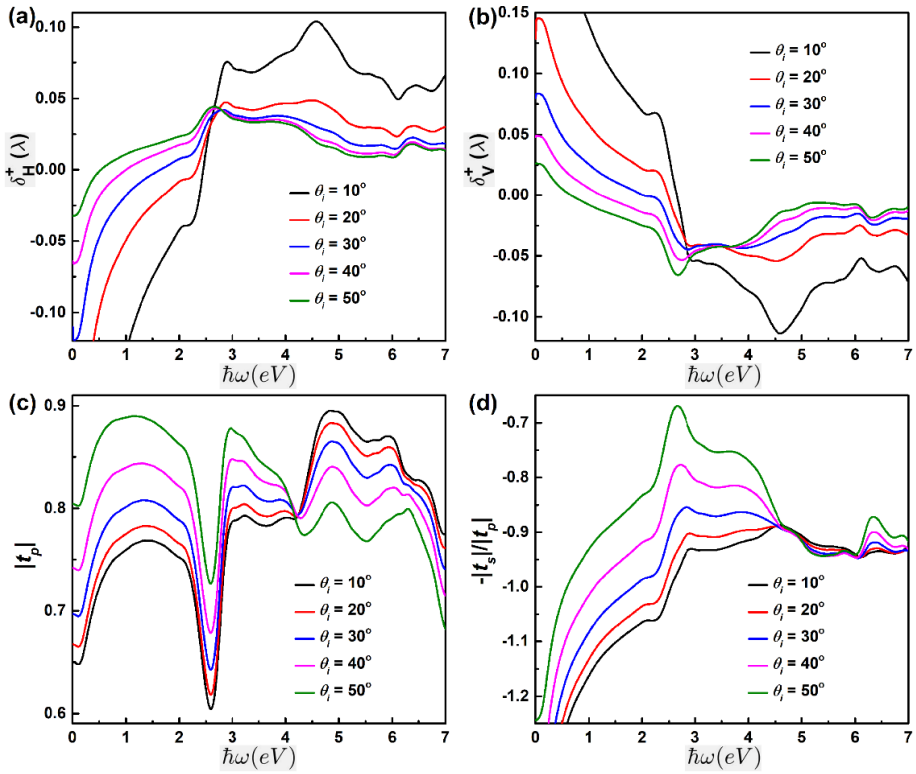

Fig. S6 Spin Hall shifts of transmitted light for (a) *H*-polarized and (b) *V*-polarized light incident on Na_3N thin film. Optical spectra of (c) transmission coefficient $|t_p|$ and (d) $-|t_s|/|t_p|$ at different incident angles. The permittivity of exit medium is set as $\varepsilon_3 = 1.0$.

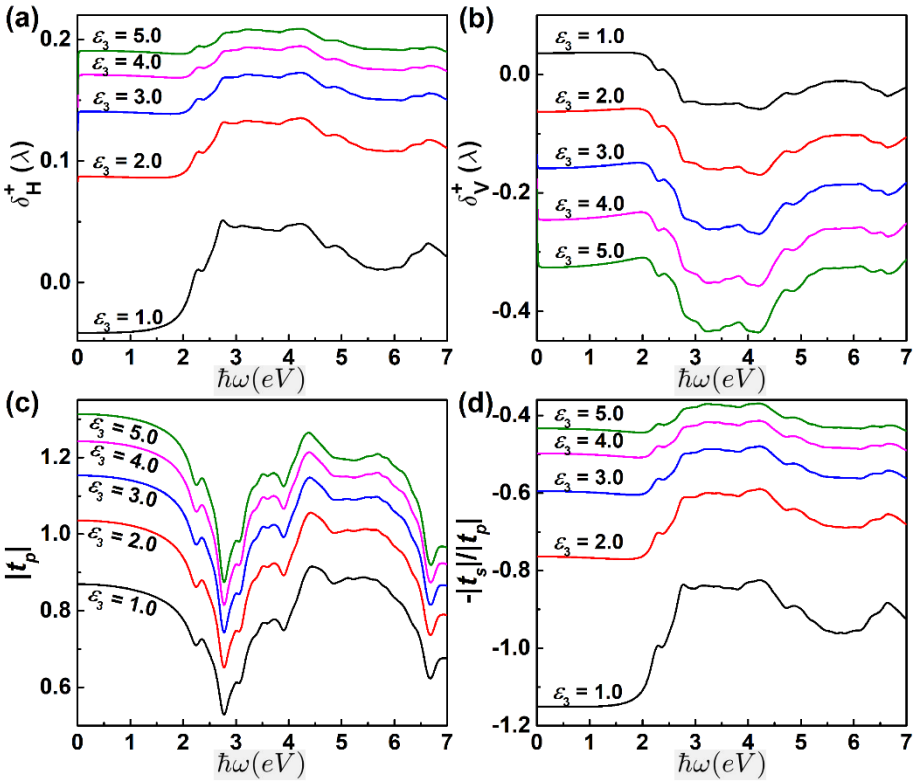

Fig. S7 Spin Hall shifts of transmitted light for (a) *H*-polarized and (b) *V*-polarized light incident on Li_3N thin film. Optical spectra of (c) transmission coefficient $|t_p|$ and (d) $-|t_s|/|t_p|$ at different permittivities of exit medium. The incident angle is set as $\theta_i = 30$ °.

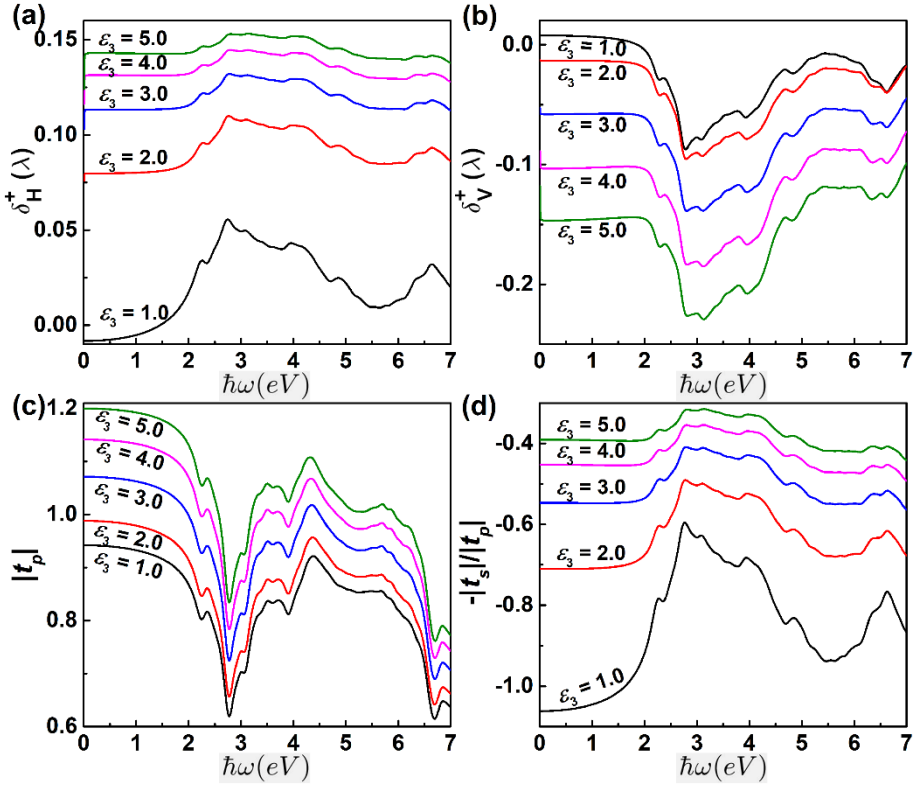

Fig. S8 Spin Hall shifts of transmitted light for (a) *H*-polarized and (b) *V*-polarized light incident on Li_3N thin film. Optical spectra of (c) transmission coefficient $|t_p|$ and (d) $-|t_s|/|t_p|$ at different permittivities of exit medium. The incident angle is set as $\theta_i = 50$ °.

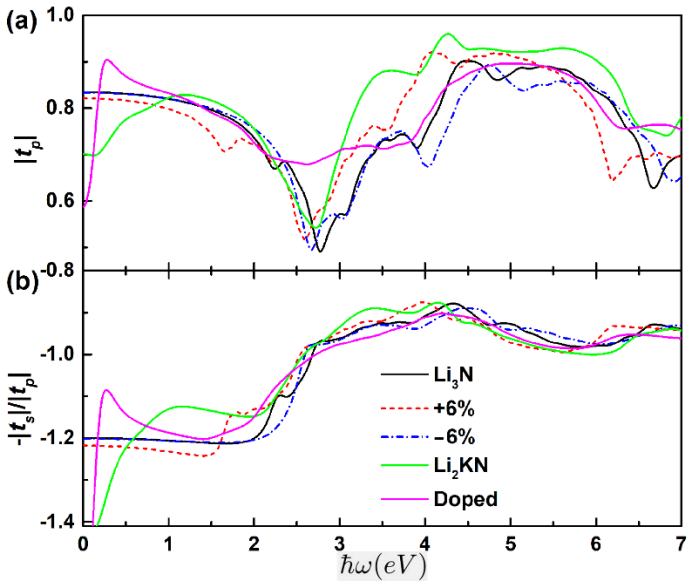

Fig. S9 Optical spectra of (a) $|t_p|$ and (b) $-|t_s|/|t_p|$ for the samples of Li_3N, +6% and -6% strained Li_3N under lattice strain along the z axis, Li_2KN, and hole-doped (0.1 holes/u.c.) Li_3N. The incident angle and the permittivity of exit medium are set as $\theta_i = 10^o$ and $\varepsilon_3 = 1.0$, respectively.

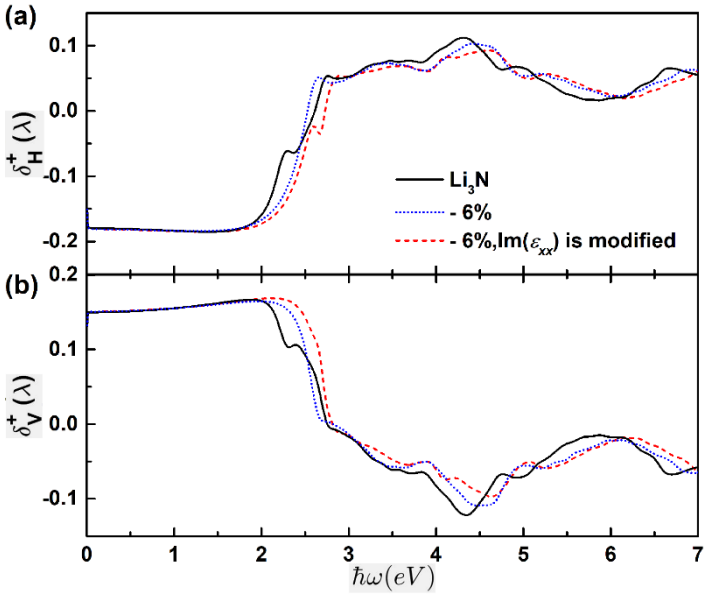

Fig. S10 Spin Hall shifts of light after artificially shifting the whole spectrum of $\mathrm{Im}(\varepsilon_{xx})$ of -6% strained Li_3N toward high-energy side by 0.2 eV, and all the other factors are the same with those for -6% strained Li_3N. For comparison, the spin Hall shifts of light for H- and V-polarized light incident on thin films of Li_3N and -6% strained Li_3N are also shown. The incident angle and the permittivity of exit medium are set as $\theta_i = 10^o$ and $\varepsilon_3 = 1.0$, respectively.

References

[1] C. Ambrosch-Draxl, S. Sagmeister, C. Meisenbichler and J. Spitaler, exciting-code, in press, http://exciting-code.org.

[2] J. P. Perdew, K. Burke and M. Ernzerhof, *Phys. Rev Lett*, 1996, 77, 3865.

[3] J. Heyd, G. E. Scuseria and M. Ernzerhof, *J. Chem. Phys.*, 2003, 118, 8207-8215.

[4] K. Hummer, J. Harl and G. Kresse, *Phys. Rev B*, 2009, 80, 115205.

[5] W. Hanke and L. J. Sham, *Phys. Rev B*, 1988, 38, 13361.

[6] G. Strinati, *La Rivista del Nuovo Cimento* (1978-1999), 1988, 11, 1-86.

[7] G. Onida, L. Reining, and A. Rubio, *Rev. Mod. Phys.*, 2002, 74, 601.

[8] P. Puschnig and C. Ambrosch-Draxl, *Phys. Rev B*, 2002, 66, 165105.

[9] M. Rohlfing and S. G. Louie, *Phys. Rev B*, 2000, 62, 4927.

[10] E. K. U. Gross and W. Kohn, *Phys. Rev Lett*, 1985, 55, 2850.